Theor Chem Acc (2005) 113: 15–27
DOI 10.1007/s00214-004-0596-x

Theoretical
Chemistry Accounts

Regular article

Ab initio calculations of vibronic activity in phosphorescence microwave double resonance spectra of *p*-dichlorobenzene

Òscar Rubio-Pons[1], Boris Minaev[2], Oleksandr Loboda[1], Hans Ågren[1]

[1]Laboratory of Theoretical Chemistry, Department of Biotechnology, The Royal Institute of Technology, AlbaNova, 10691 Stockholm, Sweden
[2]The State University of Technology, 18006 Cherkassy, Ukraine

Received: 27 May 2003 / Accepted: 27 September 2003 / Published online: 16 November 2004

Abstract. The phosphorescence spectrum of *p*-dichlorobenzene has been calculated using multiconfiguration self-consistent-field wave functions and the quadratic response technique. Attention has been paid to the intensity distribution of the singlet–triplet ($^3B_{1u}\rightarrow{}^1A_g$) transition through a number of vibronic subbands. The second order spin–orbit coupling (SOC) contribution to the spin splitting of the $^3B_{1u}$ ($^3\pi\pi^*$) state is found to be almost negligible, and the calculations therefore provide a good estimate for the zero-field splitting (ZFS) parameters based only on the electron spin–spin coupling expectation values. Nuclear quadrupole resonance constants for the different Cl isotopes are also calculated to accomplish the ZFS assignment. The electric dipole activity of the spin sublevels in the triplet–singlet transitions to the ground-state vibrational levels is estimated by calculations of derivatives using distorted geometries which are shifted from the equilibrium position along different vibrational modes. A vibrational analysis of the phosphorescence spectrum, based on the SOC-induced mixing of the singlet and triplet states calculated along different vibrational modes, provides reasonable agreement with experimental data.

Keywords: Phosphorescence microwave double resonance spectra – Vibronic activity – *p*-dichlorobenzene – Quadratic response methodology – Zero-field splitting parameters

1 Introduction

Studies of the phosphorescent state spectra of organic materials are of fundamental interest as they provide unique information on the electronic structure of molecules. The triplet state (T) has three spin sublevels which are split even in the absence of an external magnetic field; this, so-called zero-field splitting (ZFS), is determined mostly by spin-spin coupling (SSC) and is a unique characteristic of the orbital nature of the excited state. Each spin sublevel T_1^k of the lowest triplet state has its own transition probability to the ground singlet state (S_0), since it is governed by spin–orbit coupling (SOC) with specific selection rules. Moreover, each vibronic state associated with the triplet spin sublevel T_1^k utilizes a particular mechanism of intensity borrowing through SOC perturbation [1, 2].

Phosphorescence emission, $T_1\rightarrow S_0$, is known for many organic molecules [3]. Vibrationally resolved phosphorescence spectra are easily obtained for doped molecular crystals at low temperature [1,2]. Combining optical polarization measurements with studies of the Zeeman effect at a very high optical resolution, one can make assignments of the orbital, vibrational and spin symmetries of the states involved in the $T_1^k(v)\rightarrow S_0(v')$ transitions. A magnetic field additionally splits the T_1^k spin sublevels and the $T_1^k(v)\leftarrow S_0$ absorption might be expected to split into a number of separate bands [2, 3]. For example, Castro and Hochstrasser [2] have studied the Zeeman effect in the $T_1^k(v)\leftarrow S_0$ polarized absorption of a single crystal of *p*-dichlorobenzene (PDCB) at 4.2 K. The results provide important pieces of information which are not otherwise available. These are, for example, the symmetry and orbital nature of the T_1 state and of the perturbing singlet state which is mixed into T_1, and the component of the SOC operator which is most effective in the $S\rightarrow T$ mixing [2]. Additional opportunities to unravel the $T_1\rightarrow S_0$ intensity borrowing mechanisms are provided by the optically detected magnetic resonance ODMR technique [1, 4, 5, 6]. In contrast to electron paramagnetic resonance (EPR) spectra of the triplet state, the ODMR signals can be detected in zero field: a saturation of the magnetic transitions between spin sublevels leads to changes in the total equilibrium of population for the T_1 state, as well as for the excited singlet state S_1, since the rate constants for the radiative $T_1\rightarrow S_0$ transition and for nonradiative $S_1\rightarrow T_1$ and $T_1\rightarrow S_0$ transitions are strongly selective for the spin projections T_1^k. Thus, the ODMR signals can

Correspondence to: Ò. Rubio-Pons
e-mail: agren@theochem.hth.se

be observed by intensity changes in phosphorescence and fluorescence emission produced by microwaves. The mechanisms whereby the singlet-triplet transitions become allowed in phosphorescence and absorption spectra [3] become important not only for photochemistry, but also for some thermal organic reactions [7, 8], for catalysis [9], for chemically induced spin polarization [10] and for oxygen bioactivation by enzymes [11, 12].

Phosphorescence studies of the organic benchmark molecule benzene constituted a milestone in the discovery of the triplet origin of this emission [13]. Albrecht [14] confirmed the $^3B_{1u}$ assignment of the lowest triplet state of benzene by a vibrational analysis of the phosphorescence. He analyzed the possible routes for dipole-allowed $T_1^k \rightarrow S_0(v')$ transitions in benzene. Albrecht [14] concluded that the 0–0 transition is essentially forbidden (even when SOC is taken into account) and the weak phosphorescence bands originate from vibronic coupling of the e_{2g} vibrations. It is not generally possible to unambiguously assign the triplet orbital symmetry without a complete knowledge of the spin–orbit symmetries of all three spin sublevels [15]. Direct ab initio calculations of vibronic activity with account of SOC by the quadratic response technique [16, 17] supported the phenomenological analysis of Albrecht [14] and could supply a complete assignment of the vibronic phosphorescence spectrum of benzene.

In addition to benzene, substituted benzene derivatives with a more allowed character of phosphorescence have been studied by various techniques in order to support the orbital symmetry of the T_1 state and the spin–orbit symmetries of its spin sublevels [2, 3, 4, 5, 6, 8]. The PDCB molecule has received particular attention in this respect, since it belongs to a relatively high symmetry point group, D_{2h}, and contains internal heavy atoms, which enhances SOC and the $T \rightarrow S$ mixing [2, 14, 15, 19, 20, 21].

As already mentioned, the high-field Zeeman effect has been used to determine the magnitude and signs of ZFS parameters in the triplet state of the PDCB single crystal [19]. The ODMR technique has been applied to the phosphorescent triplet state of the PDCB molecule in a number of studies [4, 15, 20, 21]. Besides ZFS parameters in different crystal hosts, the ODMR methods provide electron–nuclear quadrupole and hyperfine interactions constants, the intrinsic lifetimes of individual triplet spin sublevels and their relative radiative activity in various vibronic bands present in the phosphorescence spectrum [4, 5, 20, 21, 22].

The phosphorescence of a neat PDCB crystal (spectra of excitons [5, 21] and traps [4, 15]) exhibits a long progression in the b_{2g} vibration (C–Cl bending). This indicates an out-of-plane distortion of the chlorine atoms in the phosphorescent state. The same distortion has been proposed from the observation of a large reduction in the ^{35}Cl nuclear quadrupole coupling (NQC) constant from −69.66 MHz in the S_0 state to −64.5 MHz in the T_1 state. Ab initio calculations indicate that the reduction in the chlorine NQC constant is connected with the electric field gradient change at the nucleus upon the $S_0 \rightarrow T_1$ excitation [23] and can be reproduced even in the D_{2h} point group. Castro and Hochstrasser [2] studied polarized $S_0 \rightarrow T_1$ absorption spectra and proposed that the orbital symmetry of the lowest triplet state of the PDCB molecule is B_{2u}. However, the ODMR measurements have been interpreted in terms of the B_{1u} assignment [4, 15].

Another controversial result is connected with the vibrational mode assignment. The phosphorescence of the x-trap (a shallow trap with origin at 27865 cm^{-1}) in a neat PDCB crystal exhibits a strong vibrational band at 1580 cm^{-1} [15]. This vibration originates from the e_{2g} skeletal vibrational mode of benzene (ν_8 = 1601 cm^{-1}) [17]. In benzene phosphorescence this band occurs because of strong vibronic coupling between the lowest $^3B_{1u}$ state and the second excited triplet ($^3E_{1u}$) state [6, 14, 16, 17, 24]. In the PDCB molecule the e_{2g} skeletal vibration splits into the a_g and the b_{3g} vibrational modes. In most studies the band at 1580 cm^{-1} in the PDCB phosphorescence spectrum have been assigned as being due to the a_g vibration [21]. On the basis of the ODMR signal for $T^z \rightarrow T^x$ and $T^y \rightarrow T^x$ transitions, which produces large changes in the (0,0 + 1580 cm^{-1}) band intensity of a neat PDCB crystal, Buckley et al. [15] proposed that this band is associated with both the a_g and b_{3g} vibrations, however, the optical instruments were unable to resolve these two bands. The phosphorescence microwave double resonance spectra recorded by Buckley et al. clearly indicated a big difference in responses of this band to microwave resonance saturation and that of other a_g vibronic bands; this suggests the b_{3g} assignment. At the same time, the relative radiative decay rates of the T^y and T^z sublevels are found to be incompatible with the b_{3g} origin of this phosphorescence vibronic band.

Iwasaki et al. [22] have observed optical detection of magnetic resonance signals for the deuterated PDCB phosphorescence in *p*-xylene and for the nondeuterated PDCB molecule in other hosts [21]. They showed that this band is indeed a superposition of the a_g and the b_{3g} vibrations, the frequencies of which differ from each other by only 3–4 cm^{-1} for PDCB in different hosts. In Raman spectra of deuterated PDCB the corresponding a_g and b_{3g} vibrations have been observed at 1558 and 1531 cm^{-1}, respectively.

Thus, there are many inconsistencies in the analysis of phosphorescence and ODMR spectra even for a simple benzene derivative molecule such as PDCB. Keeping in mind the successful application of ab initio analysis to spin-vibronic activity in benzene phosphorescence [16] using multiconfigurational (MC) quadratic response (QR) methodology, we apply this technique to phosphorescence and ODMR of the PDCB molecule in order to attempt to understand the origin of the previous inconsistencies for this molecule and so hopefully to increase our detailed understanding of ODMR and phosphorescence in this and other benzene derivative molecules and in general. The role of the heavy-atom effect on these spectra is then of particular interest for our present study.

2 Method of calculations

The MC self-consistent (SCF)-QR method [17, 25, 26] is used here to calculate the NQC and ZFS constants, and the electric dipole

activity of the spin sublevels in the $T_1^k \rightarrow S_0(v')$ transitions to the ground state vibrational levels of the triplet state of the PDCB molecule. Since our implementation of this model at the MCSCF level in the Dalton program [27] has already been described in previous works [23, 25, 26], we here restrict ourselves to an outline of the characteristic features of the approach. Complete-active-space (CAS) wave functions were used to compute the electronic structure in the adiabatic approximation. Relativistic corrections arising from interaction between electron spins and orbital angular momenta were added to the nonrelativistic Hamiltonian H_0:

$$H = H_0 + H_{\rm so} + H_{\rm ss} \ , \tag{1}$$

where $H_{\rm so}$ is the electronic SOC operator

$$H_{\rm so} = \frac{\alpha^2}{2}\left[\sum_{i,A} Z_A \frac{\vec{l}_{iA}\cdot\vec{s}_i}{r_{iA}^3} - \sum_{ij}\frac{\vec{l}_{ij}\cdot(\vec{s}_i + 2\vec{s}_j)}{r_{ij}^3}\right] \ , \tag{2}$$

and $H_{\rm ss}$ is the SSC operator

$$H_{\rm ss} = \frac{\alpha^2}{2}\sum_{i,j}\left[\frac{\vec{s}_i\cdot\vec{s}_j}{r_{i,j}^3} - \frac{3(\vec{s}_i\cdot\vec{r}_{i,j})(\vec{s}_j\cdot\vec{r}_{i,j})}{r_{ij}^5}\right] \ . \tag{3}$$

In general, the spin-splitting parameters D and E are determined by SSC in the first order of perturbation theory and by SOC in the second order [3].

A conventional sum-over-state expansion gives the relativistic correction matrix elements between T^i and T^j spin sublevels of the triplet reference state in the second order of perturbation theory:

$$H_{i,j} = \langle {}^3\Psi_0^i \mid H_{\rm ss} \mid {}^3\ \Psi_0^j\rangle - \sum_{n,\lambda}\sum_k \frac{\langle {}^3\Psi_0^i \mid H_{\rm so} \mid {}^\lambda\ \Psi_n^k\rangle\langle {}^\lambda\Psi_n^k \mid H_{\rm so} \mid {}^3\ \Psi_0^j\rangle}{{}^\lambda E_n - {}^3 E_0} \ . \tag{4}$$

Here ${}^\lambda\Psi_n^k$ is the zeroth-order wave function, which is an eigenfunction of the non-relativistic Schrödinger equation

$$H_0\,{}^\lambda\Psi_n^k = {}^\lambda E_n\,{}^\lambda\Psi_n^k \ , \tag{5}$$

where $\lambda = 2S + 1$ is the multiplicity of the state and S is the total spin quantum number:

$$\mathbf{S}^2\ {}^\lambda\Psi_n^k = S(S+1)\hbar^2\ {}^\lambda\Psi_n^k \ , \tag{6}$$

$$S_z\ {}^\lambda\Psi_n^k = k\hbar{}^\lambda\Psi_n^k \ . \tag{7}$$

The index $i, j, k = M_S$ determine the projection of the total spin. The SOC contribution to the ZFS of the lowest ${}^3\Psi_0$ triplet state (Eq. 4) includes singlet, triplet and quintet excited states $\lambda = 1, 3, 5$ [28]. In most cases, only the singlet-state and the triplet-state perturbations are important.

The matrix defined in Eq. (4) can be diagonalized by a principal axis transformation. For the PDCB molecule, which belongs to the D_{2h} point group, the symmetry axes of the molecular frame coincide with the magnetic axes, and the matrix Eq. (4) is thus diagonal. The eigenfunctions of the $\mid SM\rangle$ basis in Eqs. (6) and (7) can be related to the ZFS eigenfunctions by the ratios [25]

$$\mid \mathrm{T}^x\rangle = \frac{1}{\sqrt{2}}(\mid 1,-1\rangle - \mid 1,1\rangle) \ , \tag{8}$$

$$\mid \mathrm{T}^y\rangle = \frac{i}{\sqrt{2}}(\mid 1,-1\rangle + \mid 1,1\rangle) \tag{9}$$

and

$$|\mathrm{T}^z\rangle = \mid 1,0\rangle \ . \tag{10}$$

The T^k functions correspond to the zero projections of the total spin on the three molecular axes. In a coordinate system x, y, z with the ZFS eigenfunctions, Eqs. (8), (9) and (10), the effective spin Hamiltonian which describes ZFS can be written as

$$H_S = -XS_x^2 - YS_y^2 - ZS_z^2 \ , \tag{11}$$

where $X = \frac{2}{3}H_{x,x} - \frac{1}{3}(H_{y,y} + H_{z,z})$, etc. Since the ZFS tensor is traceless ($X + Y + Z = 0$) it can be presented by only two independent parameters, D and E [3]

$$H_S = D(S_z^2 - \frac{1}{3}\mathbf{S}^2) + E(S_x^2 - S_y^2). \tag{12}$$

In Eq. (12) the choice of axes is such that $\mid \mathrm{T}^z\rangle$ is the spin sublevel with the greatest splitting, i.e., ($\mid Z \mid > \mid X, Y \mid$, the z-axis being the main axis of the ZFS tensor; $D = -\frac{3}{2}Z$, and $E = \frac{1}{2}(Y - X)$.

The chlorine isotopes ^{35}Cl and ^{37}Cl have spin $I = 3/2$ and can produce hyperfine structure because of the NQC. The NQC constants are known from experiment for the ground singlet state (from the pure ^{35}Cl PDCB nuclear quadrupole resonance spectra) and for the excited triplet state of the PDCB molecule from optically detected electron–nuclear double resonance (ENDOR) [4]. By saturating the EPR transitions $T^x \rightarrow T^y$ and $T^x \rightarrow T^z$ Buckley et al. [4] observed both the ^{35}Cl ENDOR and the ^{37}Cl ENDOR resonances. Since optical properties of the phosphorescence are connected not only with the ODMR parameters, but also with this triplet resonance (optically detected ENDOR) parameters, we calculated NQC constants for both the S_0 and the T_1 states. Thus, we have to add the NQC perturbation to the nonrelativistic Hamiltonian H_0, Eq. (1) [6]:

$$H_{\rm NQC} = \sum_A \frac{eQ_A}{4I_A(2I_A-1)}\sum_i\left[\frac{\partial^2 V_i}{\partial z_{iA}^2}(3I_{Az}^2 - I_A^2) + \left(\frac{\partial^2 V_i}{\partial x_{iA}^2} - \frac{\partial^2 V_i}{\partial y_{iA}^2}\right)(I_{Ax}^2 - I_{Ay}^2)\right] \ , \tag{13}$$

where eQ_A is a nuclear electric quadrupole moment and

$$\sum_i \frac{\partial^2 V_i}{\partial z_{iA}^2} = eq_{zz} \tag{14}$$

is the electric field gradient tensor component along the main axis. The nuclear electric quadrupole moments are $Q_{\rm Cl} = -7.89 \times 10^{-26}$ e cm^2 for ^{35}Cl and $Q_{\rm Cl} = -6.21\ 10^{-2}$ e cm^2 for ^{37}Cl [29]. Other nuclei in PDCB have no spin (C), or have no quadrupole moment (H).

For the ^{35}Cl and ^{37}Cl nuclei in the PDCB molecule, the NQC operator was used in the form [4]

$$H_{\rm NQC} = \frac{1}{12}e^2 q_{zz} Q\left(3I_z^2 - \frac{9}{4}\right) \ , \tag{15}$$

where the z-axis is along the C–Cl direction (Fig. 1). In addition, the chlorine NQC asymmetry parameter

$$\eta = \frac{q_{xx} - q_{yy}}{q_{zz}} \tag{16}$$

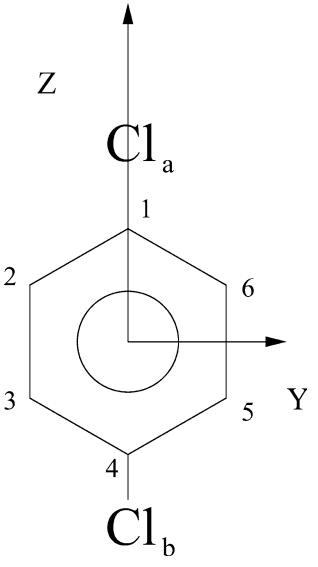

Fig. 1. Molecular structure and axis labels for *p*-dichlorobenzene. Hydrogen atoms (not shown) have the same labels as the carbon atoms to which they attach

has been neglected in Eq.(15), since its value is small in the ground state (0.08) and because η is an off-diagonal term which can not be directly measured in optiocally detected ENDOR experiments [4]. One purpose of this work is to calculate all NQC parameters and to verify the experimental results and their interpretation made by Buckley and Harris [4].

The $S \rightarrow T$ transitions are forbidden in the non relativistic approximation, but SOC mixes the spin multiplicity and gives rise to a non vanishing transition dipole moment. There have been a number of ab initio studies of the $S \rightarrow T$ transition probabilities, [23, 25, 30, 31, 32]. A typical approach is to describe the SOC perturbation in terms of a selected set of intermediate states and to perform explicit summations over the intermediate states, with a mean-field summation that is carried out over multiplet-averaged atomic orbitals. The atomic SOC integrals can be calculated efficiently owing to the high symmetry by the AMFI code [33].

The $S_0 \rightarrow T_1$ transition dipole moment (M_l) connected with a particular spin sublevel k is determined by the well-known equation

$$\begin{aligned} M_l(T^k) &= < \tilde{S}_0 \mid r^l \mid \tilde{T}_1^k > \\ &= \sum_n \frac{< S_0^0 \mid r^l \mid S_n^0 >< S_n^0 \mid H_{so}^k \mid T_1^{k,0} >}{E(T_1^0) - E(S_s^0)} \\ &\quad + \sum_m \frac{< S_0^0 \mid H_{so}^k \mid T_m^{k,0} >< T_m^{k,0} \mid r^l \mid T_1^{k,0} >}{E(S_0^0) - E(T_m^0)}, \end{aligned} \tag{17}$$

where H_{so}^k is the kth component ($k, l \in x, y, z$) of the SOC operator (T_1^0 and $\tilde{T}_1$ denote the zeroth order and first-order wave functions of perturbation theory). It is useful here to employ Cartesian triplet components (ZFS-spin functions, Eqs. 8, 9, 10).

Each k spin sublevel of the triplet state T^k is associated with a specific $S \rightarrow T^k$ transition probability. The vibronic analysis in this work is performed within the framework of the Herzberg–Teller approximation [6, 34, 35]

$$M_l^{v,v'}(T^k) = < \tilde{S}_0 v' \mid r^l \mid \tilde{T}_1^k v > \ , \tag{18}$$

where v', and v are vibrational quantum numbers for a particular vibrational mode α in the lower and upper states, respectively. The complete equation for the transition moment is

$$\begin{aligned} M_l^{v',v}(\mathrm{T}^k) &= M_l(\mathrm{T}^k)(Q_0) \int X_{\mathrm{S},v'} X_{\mathrm{T},v} dQ \\ &\quad + \frac{\partial [M_{\mathrm{S,T}}(Q)]_{Q_0=0}}{\partial Q_\alpha} \int X_{\mathrm{S}v'} Q_\alpha X_{\mathrm{T}v} \mathrm{d}Q \end{aligned} \tag{19}$$

where Q_0 is the equilibrium point geometry. In the harmonic approximation the transition moment of the 0-0 band is then given by the first term of Eq. (19) if the transition is allowed at the equilibrium geometry, as is the case for the PDCB phosphorescence. The second term is different from zero if it is excited by one vibrational quantum. In this case $\int X_{\mathrm{S}v'} Q_\alpha X_{\mathrm{T}v} \mathrm{d}Q = (h/8\pi^2 \nu_\alpha)^{1/2}$, and the total vibronic $v = 0 \rightarrow v' = 1$ transition intensity is determined by Eq. (19).

In our first approximation we shall consider the same equilibrium geometry in the upper and lower states. In that case the 0–0 band will have the Franck–Condon integral $\langle 0 \mid 0 \rangle = 1$ and the second term can be discarded because the vibrational integral will be zero in this case. For the $0 \rightarrow 1$ transition the first term will be zero in this case, because of the zero Franck–Condon integral $\langle 0 \mid 1 \rangle = 0$. Thus, we shall consider only the second term from Eq. (19) in the analysis of the vibronic progression for the α vibrational mode. This simple approximation is supported by experimental observations of the most intensive fundamental lines in the phosphorescence spectra of the PDCB molecule in different host crystals[21,22].

The derivatives of the T→S transition moment were calculated numerically for every vibrational mode. For this purpose the $^3B_{1u}(0) \rightarrow {}^1A_g(v')$ transition moments were determined for molecular geometries displaced along each individual vibrational mode α using a step size of $\Delta Q_\alpha = 0.8$ amu$^{1/2}$ Å.

For the vibronic $0 \rightarrow 1$ phosphorescence $^3B_{1u}(v = 0) \rightarrow {}^1A_g(v' = 1)$ transition band emitted from a ***k***-spin sublevel the transition moment is (in atomic units)[36]

$$M_{\mathrm{ST}^{k0,1}} = \frac{\partial [M_{\mathrm{ST}^k}(Q)]_{Q_o}}{\partial Q_\alpha} (2\pi \nu_\alpha)^{-1/2} \ . \tag{20}$$

The lifetime (τ) of a given spin sublevel k for a given vibrational mode α is equal to:

$$\frac{1}{\tau_k} = \kappa_k = \frac{4\omega_e^3 \gamma^3}{3t_0} \left[\frac{\partial [M_{\mathrm{ST}^k}(Q)]_{Q_0}}{\partial Q_\alpha} \right]^2 (2\pi \nu_\alpha) \ , \tag{21}$$

where $t_0 = \frac{(4\pi\varepsilon_0)^2 \hbar^3}{m_e e^4} = 2.4189 \cdot 10^{-17}$s, γ is the fine-structure constant, $\gamma \approx \frac{1}{137}$, κ_k is the radiative decay constant, and ω_e is the transition energy between the zero-vibrational level of the triplet state and the vibrational level $v = 1$ for the mode α of the ground state.

It was noted in Refs. [6, 30, 32] that convergence of the S→T transition moment (Eq. 17) in a configuration interaction treatment is very slow. Many terms in the sum-over-state expansion (Eq. 17) are of similar magnitude but of different signs [6, 25]. In response theory [25] the matrix element of Eq. (17) is associated with the residue of a QR function at the excitation frequency of the S→T transition. The sum-over-state expression (Eq. 17) in MCSCF-QR theory of the S→T transition moment is replaced by solutions of sets of linear equations [25]. Since these solutions can be determined using direct iterative techniques of the response equations, large dimensions and therefore large orbital and configuration space MCSCF wave functions can be considered. This permits us to calculate electric dipole activity of all spin sub-levels T_1^k of such a relatively large molecule like PDCB with displacements along all vibrational modes.

2.1 Basis sets and active spaces

A number of active spaces and basis sets were employed in the present study. On the basis of precalculations of these as well as on experience with previous calculations on ODMR and phosphorescence spectra, in particular for the benzene molecule, we decided to present results using the following parameterization (for the active space this is further substantiated by bonding and natural occupation number analysis:
Atomic natural orbitals basis sets [37] were used for all atoms. These are C (14s4p4d), Cl (17s12p5d), and H(8s4p) contracted to C {4s3p1d}, Cl {5s4p3d}, H {2s1p}. The CAS was composed of 14 electrons and 12 orbitals [CAS (14/12)]. With this CAS (14/12) the optimization of the ground state, keeping D_{2h} symmetry, and the calculation of NQC, were done. The active space was composed of π orbitals from the benzene ring (six π), and the two chlorine atoms (four π), and the two σ orbitals from the bond between carbon and chlorine [four σ_{Cl-C}, CAS (14/12)] included with the corresponding antibonding counterparts to complete the active space.

In the calculations of the singlet–triplet transition dipole moments, and of the energies of every vibrational mode, the active space was reduced to ten electrons and ten orbitals [CAS (10/10)] keeping inactive the deepest orbitals from the active space CAS (14/12) using the analysis of the natural occupation numbers. With this new active space [CAS (10/10)] the NQCs were calculated as well.

2.2 Geometry optimization

The PDCB molecule was placed in the ***zy***-plane, where the z axis is the long axis containing the two chlorine atoms, and the y-axis is the short axis. A scheme of the molecule and the atom labels are presented in Fig. 1. The ground-state geometry optimization and the calculation of the vibrational frequencies were carried out using CASSCF analytic gradients including 14 electrons and 12 orbitals in the active space; CAS (14/12). The geometry optimization was constrained to D_{2h} symmetry. With the optimal geometry from the CAS (14/12) calculation a second optimization procedure was carried out to check the frequencies and the geometrical parameters, using density functional theory (DFT) at the B3LYP/6-31G* level to clarify the ground-state geometry. No large differences were found for the ground state, so the geometry from the CASSCF optimization was used.

The geometry of the lowest triplet excited state of PDCB was optimized in several steps, in D_{2h}, C_s and C_{2h} symmetry restrictions

and without any symmetry requirements at the B3LYP/6-31G* level.

All calculations were carried out with the DALTON quantum chemistry package [27], except the DFT geometrical optimizations, which were done with the GAUSSIAN 98 package [38].

3 Results and discussion

From the conceptual background of ODMR methodology in phosphorescence studies, it follows that optical and magnetic properties of the triplet state are closely connected. The ZFS constants D and E of the spin Hamiltonian (Eq. 12) can give important information about the symmetry and electronic structure of the triplet state. On the other hand, transition intensities and the polarization of the phosphorescence emission from separated spin sublevels can be analyzed with account of magnetic perturbation of the electronic wave functions being ingredients of the spin alignment of the zero-field sublevels.

ODMR spectra recorded by monitoring all vibronic lines in the $T_1^k \rightarrow S_0(v_i)$ emission is called the phosphorescence microwave detected resonance (PMDR) in the literature [5]. The ab initio response technique has proved very useful for the direct interpretation of PMDR spectra [25]. Perturbations produced by vibrational movement are connected with magnetic interactions and with UV optical activity; thus intensities of vibronic lines from each spin sublevel provide additional criteria to unravel the correlation between optical and magnetic properties of the triplet state [36]. Ab initio calculations of the PDCB molecule using the MCSCF QR method present an exhaustive example of such a theoretical analysis. We present here results for structural changes upon the singlet–triplet vibrational excitation, $T_1^k \rightarrow S_0(v')$ transition moments, frequencies and NQC properties. All the data are collected in Tables 1, 2, 3, 4, 5 and 6.

The calculated fundamental vibrational modes are presented and compared with the experimental modes in Table 1, the geometries for the singlet and triplet states are presented in Table 2 and the NQC results are collected in Table 3. The transition moments for the vibrational modes, the vibrational frequencies v_α and the assignments of the modes are given in Tables 4, 5 and 6. The total lifetimes for the different spin sublevels and different vibrational modes are also included.

We calculated the vertical excitation $T_1^k \leftarrow S_0$ spectrum of PDCB as the first approach to assign the phosphorescence bands. It was shown [2] that the Franck–Condon maximum in the long b_{2g} progression is located at about $n = 1$ to $n = 3$; thus, the triplet state symmetry is not severely modified from the D_{2h} point group. Following the analysis of Castro and Hochstrasser [2] we expect SOC selection rules to be subject to the same restrictions, namely, that most of the spectrum will appear via the D_{2h} selection rules, and the effect of distortion would be small.

For the choice of axes given in Fig. 1 the lowest triplet state in the PDCB molecule is the $^3B_{1u}$ ($^3\pi\pi^*$) state. The SSC-induced D value can be determined by the x-axis: $D = (-3/2)\ X = 0.164\ \text{cm}^{-1}$ [23], in good agreement with the experimental D value ($0.144\ \text{cm}^{-1}$) for the x-trap in a neat crystal and the same choice of the main axis [4]. The SOC contribution for parameter D is found to be less than $10^{-2}\ \text{cm}^{-1}$ and for parameter E less than $10^{-3}\ \text{cm}^{-1}$. Thus, the internal heavy-atom effect is not important for ZFS in the PDCB molecule.

The positive sign of D is clearly brought out from studies of the optical Zeeman effect [40] and from ODMR studies [4, 15, 21, 20]. The choice of presentation of the E parameter is rather arbitrary. Following the general convention, we earlier used a definition $E = \frac{1}{2}(Y - Z)$ [23], since for the PDCB molecule (Fig. 1) this is just an interchange of Z and X parameters in comparison with the standard choice in Eq. (12). But in the work of Buckley et al. [4] the ZFS definition contradicts the general convention for E. They used the definition

$$E = \frac{1}{2}(Z - Y)\ , \tag{22}$$

Table 1. Fundamental vibrations identified in the phosphorescence spectrum of the (PDCB) molecule in different crystal hosts together with the Raman spectrum of the D_{2h} ground state. Theoretical results are from (CASSCF) (14/12) calculations. The frequencies are given in reciporcal centimeteres

Symmetry	Theoretical		Experimental[a]			
	Mode	v_α	Raman	*p*-Xylene	Neat crystal	PDCB-d_4
a_g	v_1	3371.37	3071	–	–	–
b_{3g}	v_3	3354.54	3064	–	–	–
a_g	v_5	1713.61	1577	1577	1578	1555.7
b_{3g}	v_6	1692.73	1577	1573	1581	1549.6
b_{3g}	v_9	1413.13	1293	1297	1292	1018.2
a_g	v_{10}	1265.92	1174	1171	1180	1082.4
a_g	v_{14}	1132.58	1103	1098	1108	866.8
b_{2g}	v_{17}	976.36	976	938	938	793.0
b_{1g}	v_{19}	846.54	814	821	818	639.8
a_g	v_{20}	775.78	744	751	746	711.6
b_{2g}	v_{21}	713.07	689	694	691	606.7
b_{3g}	v_{22}	673.72	628	637	636	–
b_{3g}	v_{26}	364.81	350	–	355	327.4
a_g	v_{27}	333.81	327	–	333	327.4
b_{2g}	v_{28}	295.01	306	303	314	295.6

[a]Experimental data in different matrices, from Refs: 21, 22

Table 2. Geometry parameters in the ground and triplet states of PCDB optimized with different symmetry restrictions. The bond lengths (R) are in angstrom and the plain (L) and dihedral (<) angles are in degrees

Parameters	1^1A_g[a]	1^1A_g[b]	$1^3A'$[a]	1^3B_u[a]	1^3B_{1u}[a]
$R(C_1-C_2)$	1.395	1.389	1.428	1.465	1.416
$R(C_2-C_3)$	1.395	1.392	1.364	1.352	1.434
$R(C_3-C_4)$	1.394	1.389	1.472	1.465	1.416
$R(C_4-C_5)$	1.394	1.389	1.472	1.464	1.416
$R(C_5-C_6)$	1.395	1.392	1.364	1.352	1.434
$R(C_6-C_1)$	1.394	1.389	1.428	1.464	1.416
$R(C_1-Cl_a)$	1.757	1.769	1.738	1.748	1.731
$R(C_4-Cl_b)$	1.757	1.769	1.830	1.748	1.731
$R(C_2-H_2)$	1.085	1.072	1.086	1.085	1.081
$R(C_3-H_3)$	1.085	1.072	1.086	1.085	1.081
$R(C_5-H_5)$	1.085	1.072	1.086	1.085	1.081
$R(C_6-H_6)$	1.085	1.072	1.086	1.085	1.081
$\angle(C_6C_1C_2)$	121.055	121.306	121.644	119.225	125.550
$\angle(C_2C_1Cl_a)$	119.471	119.347	119.078	117.477	117.225
$\angle(C_3C_4C_5)$	121.056	121.306	117.373	119.225	125.550
$\angle(C_3C_4Cl_b)$	119.470	119.347	112.726	117.477	117.225
$\langle(Cl_aC_1C_2C_3)$	179.963	180.000	179.767	151.3934	180.000
$\langle(Cl_bC_4C_3C_2)$	179.982	180.000	112.295	151.3934	180.000

[a]B3LYP/6-31G* optimized geomentry
[b]CASSCF(14/12) optimized geomentry

Table 3. Theoretical resonance nuclear quadrupole coupling parameters (MHz) for the lowest triplet state of the PDCB molecule in D_{2h} and C_{2h} symmetry calculated at different CASSCF levels

Symmetry	X	CAS	η	$e^2q_{xx}Q_X$	$e^2q_{yy}Q_X$	$e^2q_{zz}Q_X$
C_{2h}	^{35}Cl	14/12	0.1094	29.813	37.138	−66.951
	^{37}Cl			23.496	29.269	−52.765
C_{2h}	^{35}Cl	10/10	0.1219	29.312	37.455	−66.766
	^{37}Cl			23.101	29.519	−52.620
D_{2h}	^{35}Cl	14/12	0.1332	29.061	37.995	−67.056
	^{37}Cl			22.903	29.445	−52.848
D_{2h}	^{35}Cl	10/10	0.1216	29.080	37.132	−66.213
	^{37}Cl			22.919	29.265	−52.184

and other authors [15, 20, 21] also follow this trend. Thus, we get the E parameter to be negative in agreement with ODMR experimental data [4, 15, 20, 21]. The calculated E value ($E = -0.024$ cm^{-1}) perfectly fits the experimental result ($E = -0.023$ cm^{-1}) [4, 23].

The NQC tensor was calculated for both ^{35}Cl and ^{37}Cl NQC-active isotopes by the MCSCF method for optimized geometries in the singlet ground state and in the first triplet state. In the S_0 state the calculated NQC constant [23] for the main axis (z, the direction of the C–Cl bonds) and for the ^{35}Cl-containing PDCB molecule is $e^2q_{zz}Q_{35} = -71.94$ MHz, while the asymmetry parameter is small indeed, $\eta = 0.06$, in good agreement with the experimental value $\eta = 0.08$ [4].

The measured pure nuclear quadrupole resonance frequency of the PDCB molecule (with the ^{35}Cl isotopes) in its ground state at 4.2 K is $\nu = 34.83$ MHz [4]. A similar value (34.78 MHz) is given by Lucken [41] for a crystal at 77 K. If η is assumed to be zero, this resonance frequency corresponds to a value of $e^2q_{zz}Q_{35} = -2\,\nu = -69.66$ MHz. The assumption that η may be neglected is justified on the basis that $e^2q_{zz}Q$ is not changed significantly for small values ($\eta \approx 0.1$) [4,41]. The calculated result for the complete NQC tensor supports all these assumptions (Table 3).

For the purpose of our study the most important result is connected with the NQC constant reduction upon the $T_1 \leftarrow S_0$ excitation. For the D_{2h}-optimized geometry in the T_1 state we get $e^2q_{zz}Q_{35} = -67.06$ MHz and $\eta = 0.1332$, which is in good agreement with the experimental value of −64.5 MHz [4].

Thus the absolute value of the main NQC component is reduced by 5.16 MHz in the nuclear quadrupole resonance measurements upon the $T_1 \leftarrow S_0$ excitation of a neat PDCB crystal at 4.2 K. Our MCSCF calculations predict a similar reduction by 4.88 MHz. This reduction of the magnitude in the $|e^2q_{zz}Q|$ value upon the $T_1 \leftarrow S_0$ excitation is quite big, it is much larger than for 8-chloroquinoline and for *sym*-tetrachlorobenzene [4], which also have the lowest triplet state of $\pi\pi^*$ nature. The absolute value $|e^2q_{zz}Q|$ in the T_1 state of PDCB is significantly smaller than the values reported for any chlorine-containing aromatic molecule in the ground state [4, 41].

As pointed out in the work of Buckley et al. [4], the small increase of 0.05 MHz in the pure nuclear quadrupole resonance frequency of the ground-state PDCB molecule upon cooling the sample from 77K (34.78 MHz) to 4.2 K (34.83 MHz) is consistent with the quenching of the PDCB torsional motions in the crystal. This very small increase of the NQC constant indicates negligible effects of intermolecular interactions in the crystal on the field gradient at the ^{35}Cl nuclei and, probably, on the whole electronic shell. Buckley et al. [4] tentatively interpreted the change in the $e^2q_{zz}Q_{35}$ value upon $T_1 \leftarrow S_0$ excitation in the PDCB molecule as arising

Table 4. Transition moments $M_i(T^k)$ and their derivatives $M_i'(T^k)$ from the T^y and T^x spin sublevels, and their partial rate constants (κ^i,s^{-1}) from the total symmetric modes a_g in PDCB phosphorescence. All the transition moments and their derivatives are multpliled by 10^6 (in atomic units)

Symmetry	Mode	ν_α(cm^{-1})	$M_y(T^x)$	$M_x(T^y)$	$M_y'(T^x)$	$M_x'(T^y)$	κ^ys^{-1}	κ^xs^{-1}
a_g	ν_1	3371.37	−2.01	−4.23	−0.63	−1.25	0.0006	0.0001
a_g	ν_5	1713.61	0.00	22.57	0.00	5.00	0.0188	0.0000
a_g	ν_{10}	1265.92	−3.28	−13.13	−0.63	−2.50	0.0064	0.0004
a_g	ν_{14}	1132.58	−3.47	3.47	−0.63	0.63	0.0005	0.0005
a_g	ν_{20}	775.78	−4.19	0.00	−0.63	0.00	0.0000	0.0007
a_g	ν_{27}	333.81	0.00	6.39	0.00	0.63	0.0015	0.0000

Table 5. Transition moments $M_i(T^k)$ and their derivatives $M_i'(T^k)$ from the T^z and T^xspin sublevels, and their partial rate constants (κ^i) for the modes of b_{3g} symmetry in PDCB phosphorescence. All the transition moments and their derivatives are multpliled by 10^6 (in atomic units)

Symmetry	Mode	$\nu_\alpha(cm^{-1})$	$M_z(T^x)$	$M_x(T^z)$	$M_z'(T^x)$	$M_x'(T^z)$	$\kappa^x s^{-1}$	$\kappa^z s^{-1}$
b_{3g}	ν_3	3354.54	2.01	4.033	0.63	1.25	0.0002	0.0006
b_{3g}	ν_6	1692.73	11.35	39.75	2.50	8.75	0.0048	0.0582
b_{3g}	ν_9	1413.13	3.11	15.54	0.63	3.13	0.0004	0.0089
b_{3g}	ν_{22}	673.72	4.50	4.50	0.63	0.63	0.0007	0.0007
b_{3g}	ν_{26}	364.81	6.11	6.11	0.63	0.63	0.0014	0.0014

Table 6. Transition moments $M_i(T^k)$ and their derivatives $M_i'(T^k)$ from the T^y and T^z spin sublevels, and their partial rate constants (κ^i) for the modes of b_{2g} symmetry in PDCB phosphorescence. All the transition moments and their derivatives are multpliled by 10^6 (in atomic units)

Symmetry	Mode	$\nu_\alpha(cm^{-1})$	$M_z(T^y)$	$M_y(T^z)$	$M_z'(T^y)$	$M_y'(T^z)$	$\kappa^y s^{-1}$	$\kappa^z s^{-1}$
b_{2g}	ν_{17}	976.36	3.36	14.95	0.63	2.50	0.0418	0.0083
b_{2g}	ν_{21}	713.07	5.69	4.37	8.13	5.63	0.1194	0.0007
b_{2g}	ν_{28}	295.01	136.01	20.40	12.50	1.88	0.6831	0.0154

from the out-of-plane bending of the C–Cl bond. Our calculations of the planar PDCB molecule (D_{2h} point group) indicate that the main contribution to the NQC constant change is entirely due to a change in the electric field gradient upon excitation. The optimized C–Cl bond length in the S_0 and T_1 states is 1.769 A and 1.737 Å, respectively. The C–Cl bond gets stronger upon excitation, see Table 2.

In summary, from the electronic and nuclear spin state splitting of the phosphorescent state one can conclude that the chlorine atoms have an appreciable influence on the space distribution of the $\pi\pi^*$ electrons. They strongly influence the ZFS parameter E but change the D parameter only slightly in comparison with the benzene molecule. The change of the nuclear quadrupole resonance frequency upon the $T_1 \leftarrow S_0$ excitation indicates that spin-dependent magnetic interactions would strongly modify the phosphorescence of the PDCB molecule as compared with benzene phosphorescence.

3.1 Conformations of the singlet and triplet states

The first excited triplet state is predicted in our CASSCF-QR calculations to have $^3B_{1u}$ symmetry in the D_{2h} point group. At the same time we obtained two imaginary vibrational frequencies, indicating that the D_{2h} structure does not correspond to the global minimum for the T_1 state. This is in agreement with the occurrence of a long progression of the b_{2g} vibrational mode (ν = 303 cm^{-1}) in the phosphorescence spectrum. Our DFT calculations without symmetry restrictions indicate that the optimal geometry of the triplet state has the structure with one C–Cl bond out of the plane.

At this geometry the molecule possesses a reflexion plane containing both C–Cl bonds, with the molecule belonging to the C_s group, see Fig. 2. At this geometry one of the chlorine atoms is in the benzene ring plane and the other one is out of the plane with a dihedral angle of 112. 29°, and with a longer C–Cl bond distance, see Table 2. This structure will give two different NQC constants, something that contradicts the observed fine structure of the optically detected ENDOR spectrum. The energy difference between the triplet geometry at the C_s final geometry and the restricted structure in D_{2h} is quite large, approximately 1 eV.

To provide an equivalent electronic structure for the two chlorine atoms a constraint-symmetry calculation was implemented for the PDCB triplet state. We restricted the geometry to D_{2h}, C_{2h} and C_{2v} points groups. In the case of C_{2v}, the molecule possesses a boat conformation and higher energy, owing to the electronic repulsion of the two chlorine atoms, in comparison to the lowest triplet state at D_{2h} geometry. The C_{2h} structure, with the two Cl atoms pushed out of plane in the trans configuration is more stable than the D_{2h} structure by 0.83 eV, Fig. 3, but one imaginary frequency appeared, and this structure should therefore correspond to a transition state between C_s minima. In the case of

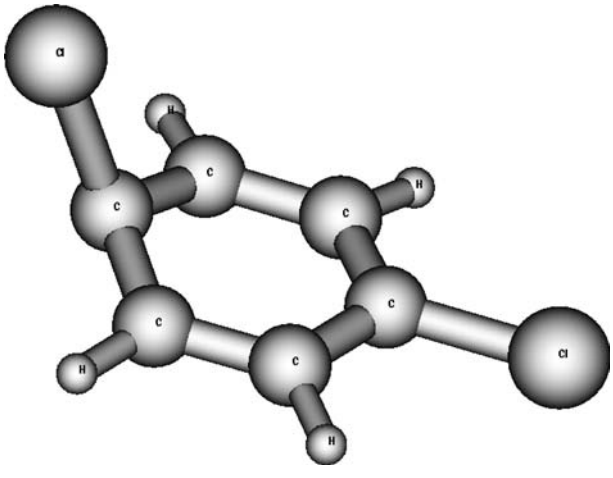

Fig. 2. Molecular structure of the triplet state of *p*–dichlorobenzene optimized in C_s symmetry

the C_{2h} structure, the NQC constant $| e^2q_{zz}Q |$ is 66.95 MHz, with CAS (14/12), the value of $\eta = 0.1094$, and the difference with the triplet state at D_{2h} symmetry is only 0.105 MHz. This reduction of the $| e^2q_{zz}Q |$ value is almost negligible in comparison with the value for the ground state $| e^2q_{zz}Q | = 71.94$ MHz. It is clear that the total reduction of about 5MHz is related to the electric field gradient change during the S→T transition.

The C_{2h} triplet-state structure is only 0.15 eV higher than the C_s minimum, but constitutes nevertheless a large geometric distortion from the global minimum (C_s) point with two distinct electronic structures for the chlorine atoms. Such a large distortion should though not be present in the matrix crystal owing to the pressure that the crystal makes. Probably, the crystal force fields do not permit the molecule to accept the most favorable geometry. In real systems, the deformation seems to be connected with the crystal field perturbation and, probably, with excimer formation. This follows from the fact that the emission spectrum is more perturbed by the crystal field than the absorption [2]. In their work on the $T_1 \leftarrow S_0$ absorption spectra of single crystals Castro and Hochstrasser [2] argued that most of the spectral intensity appears via D_{2h} selection rules and that the effect of the distortion is small.

In the C_{2h} geometry the imaginary frequency corresponds to the trans–symmetrical bending movement of the chlorine atoms in the x-axis, trying to reach a similar structure as the C_s symmetry. Thus the C_{2h} structure corresponds to a transition state if we consider the trans–symmetrical bending as the reaction coordinate for the left–right isomerization of the C_s species shown in Fig. 2. In Fig. 3 we have described a qualitative scheme of the potential energy surfaces for the lowest triplet state optimized with different symmetry constraints. In this case, the lower potential energy surface for the triplet state presents two symmetrical minima corresponding to the triplet structures distorted along the reaction coordinate.

The change in electric field gradient upon the S→T transition is almost reproduced at the D_{2h} symmetry

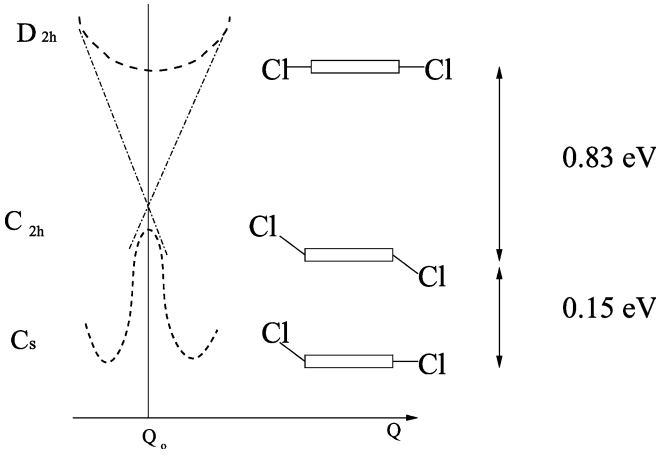

Fig. 3. Energy differences of the optimized *p*-dichlorobenzene structures together with the scheme of the potential energy surfaces for the lowest triplet state assuming several symmetry restrictions

restriction. The nonsymmetrical optimized structure of the PDCB molecule in the triplet state is strongly distorted with one C–Cl bond being far out of plane; this structure is only slightly stables than the C_{2h} structure and cannot be realized in the crystal. The D_{2h} and C_{2h} structures have similar C–Cl bond lengths (Table 2) in the triplet state, both being shorter than in the ground singlet state. Since the C–C bond lengths are quite different in the two triplet-state C_s structures, one can see that the frequencies of the vibronic bands in the $T_1 \rightarrow S_0$ emission are determined by the ground-state D_{2h} force field and the intensities of the fundamental vibronic bands in the $T_1 \rightarrow S_0$ emission are determined mostly by the D_{2h} symmetry selection rules, since the triplet-state wave function reproduces the same main features in the D_{2h} structure. From comparison of our calculations with the experimental NQC tensors in the ground and in the first excited triplet states of the PDCB molecule in different crystal hosts we conclude that the geometry changes do not have a big influence on the NQC parameters. Even the vertical $T_1 \leftarrow S_0$ excitation produces an appreciable reduction of the $| e^2q_{zz}Q |$ parameter in qualitative agreement with the observed NQC frequency. For all these reasons we consider the vertical transition as the source of the main phosphorescence in the D_{2h} structure and the intensity of the fundamental vibronic bands obtained by derivatives (Eq. 20) calculated for the ground-state vibrational modes with the D_{2h} equilibrium.

3.2 Vibronic bands

The vibrational phosphorescence spectrum of PDCB consists mostly of three principal groups of bands originating from several intense vibronic modes; these bands are presented in the interval of frequencies between the 0,0 band and 0,0 + 1580 cm^{-1}, see Fig. 4. The spectrum is formed by the 0,0 band ($\nu_{0,0}$) and its subsequent components, the strongest group of which resides at about 300 cm^{-1} with three vibrational modes, ν_{28}, ν_{26} and ν_{27}. The most studied group is at about 1700 cm^{-1} and consists of two modes ν_5 and ν_6 (it is cited in Refs: [21, 22] as the band at about 1580 cm^{-1}). In the higher region of the spectrum (about 3300 cm^{-1}) two vibrational bands occur with very low intensity. They are not well resolved and have not been properly studied in the experimental spectra, but are nevertheless presented in our theoretical data. These are assigned to ν_1 and ν_3, see Table 1 and Figures 4, 5 and 6 for more details.

In the first approximation we consider the vertical $T_1 \leftarrow S_0$ transition as a model for the 0,0 band. The square of the $T_1 \leftarrow S_0$ transition moment has to be multiplied by the Franck–Condon factor calculated for the 0,0 band determined by gradients from the MCSCF geometry optimization in D_{2h} symmetry. We consider that all three spin sub-levels have the same potential energy surfaces, since geometry optimization is carried out by a nonrelativistic approach. This assumption is evidently not correct in general; the SOC-induced mixing between excited S and T states and between triplet T_1^k

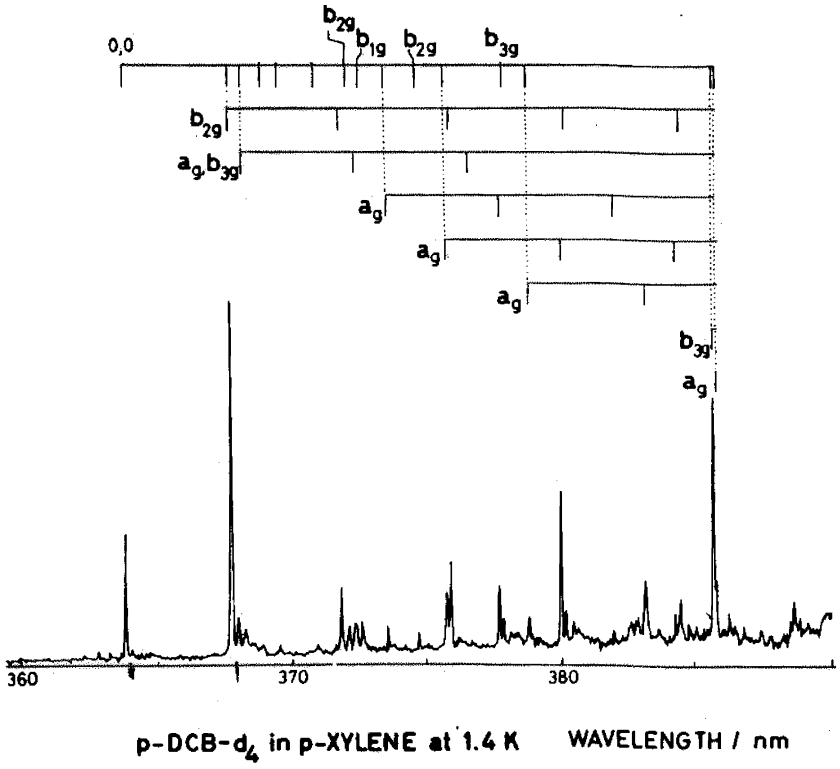

Fig. 4. Experimental phosphorescence spectrum of *p*-dichlorobenzene in *p*–xylene at 1.4K. The *uppermost bar* shows the fundamentals vibrations. Taken from Ref [22] with permission of Elsevier

and T_n^k states with different potential energy surfaces (gradients) produces small contributions that make vibrational frequencies and equilibrium geometries differ slightly for the three spin substates. At the moment we can only neglect such possible spin-selective distortions. All the spin sublevels are calculated at the S_0 optimized geometry under the assumption that the Franck–Condon factor is 1 for the 0,0 transition. As follows from our MCSCF-QR calculations the 0,0-band is present at 3.26 eV. The $T_1 \rightarrow S_0$ transition has a large transition probability from the T^y spin sublevel and is *x*-polarized $[M_x(T^y) = 148\times10^{-6} au]$. The radiative rate constant for this emission from spin sublevel T^y is $\kappa^y = 0.8088\ s^{-1}$. The 0,0 phosphorescence band originating from the T^x spin sublevel is less intensive and has *y* optical polarization ($\kappa^x = 0.0213\ s^{-1}$).

Any changes in phosphorescence intensity while monitoring the emission to a vibrational level of the ground state indicate differences in the transition probability from different spin sublevels of the T_1 state induced by these vibrations. We used vibrational modes calculated for the ground state to monitor the changes induced in SOC and in vibronic activity of the spin sublevels. As already mentioned in the Introduction, the most striking feature of the phosphorescence microwave double resonance spectra of the PDCB crystal is a relative increase in intensity of the vibronic band (0,0 + 1580 cm^{-1}) upon the $T^z \rightarrow T^x$ microwave transition saturation and a strong decrease upon the $T^y \rightarrow T^x$ microwave resonance [15].

Geometry optimization of the ground state, performed at the MCSCF, level indicates that the analogue of the benzene e_{2g} skeletal vibrational mode (ν_8 = 1601 cm^{-1}) [17] is split in the PDCB molecule as $a_g(\nu_5$ = 1713.61 cm^{-1}) and $b_{3g}(\nu_6$ = 1692.73 cm^{-1}) vibrations. Experimental data for the neat crystal predict these two modes to be almost degenerate at 1580 cm^{-1} [15]. Our MCSCF-QR calculations show that the T^y spin sublevel gets more emissive upon involvement of the $a_g(\nu_5)$ vibration in the lower state. The derivative is quite big, $M' = \partial M(T^y)/\partial Q_{1731} = 0.000005$. The κ^x/κ^y ratio for the (0,0 + 1580 cm^{-1}) vibronic band of the a_g type is also changed in comparison with the 0,0 band. In benzene phosphorescence this band occurs because of strong vibronic coupling between the lowest $^3B_{1u}$ state and the second excited triplet ($^3E_{1u}$) state [6, 14, 16, 17, 24]. In most works the band at 1580 cm^{-1} in the PDCB phosphorescence spectrum has been assigned as being due to the $a_g(\nu_5)$ vibration [21]. On the basis of ODMR signal for $T^z \rightarrow T^x$ and $T^y \rightarrow T^x$ transitions, which produces great changes in the (0,0 + 1580 cm^{-1}) band intensity of a neat PDCB crystal, Buckley et al. [15] have proposed that this band is associated with both the a_g and the b_{3g} vibrations.

We obtain the ratio of the radiative rate constants, $\kappa^x/\kappa^y = 0.0263$, in reasonable agreement with the experimental value of 0.026, obtained for the 0,0 band ($\nu_{0,0}$) phosphorescence band of PDCB in a benzene host crystal at 1.4 K [21]. The change of the κ^x/κ^y ratio for the a_g (0,0 + 1580 cm^{-1}) vibronic band is due to an increase of the contribution in the spin sublevel T^y and because there is no active contribution from the spin sublevel T^x, as follows from our calculation, see Table 4. This is in a good agreement with the microwave-induced delayed phosphorescence (MIDP) spectra [21]. In the MIDP spectrum the phosphorescence of PDCB is resolved into two magnetic spin sublevel spectra. The T^y spectrum is recorded by phase-sensitively detecting the

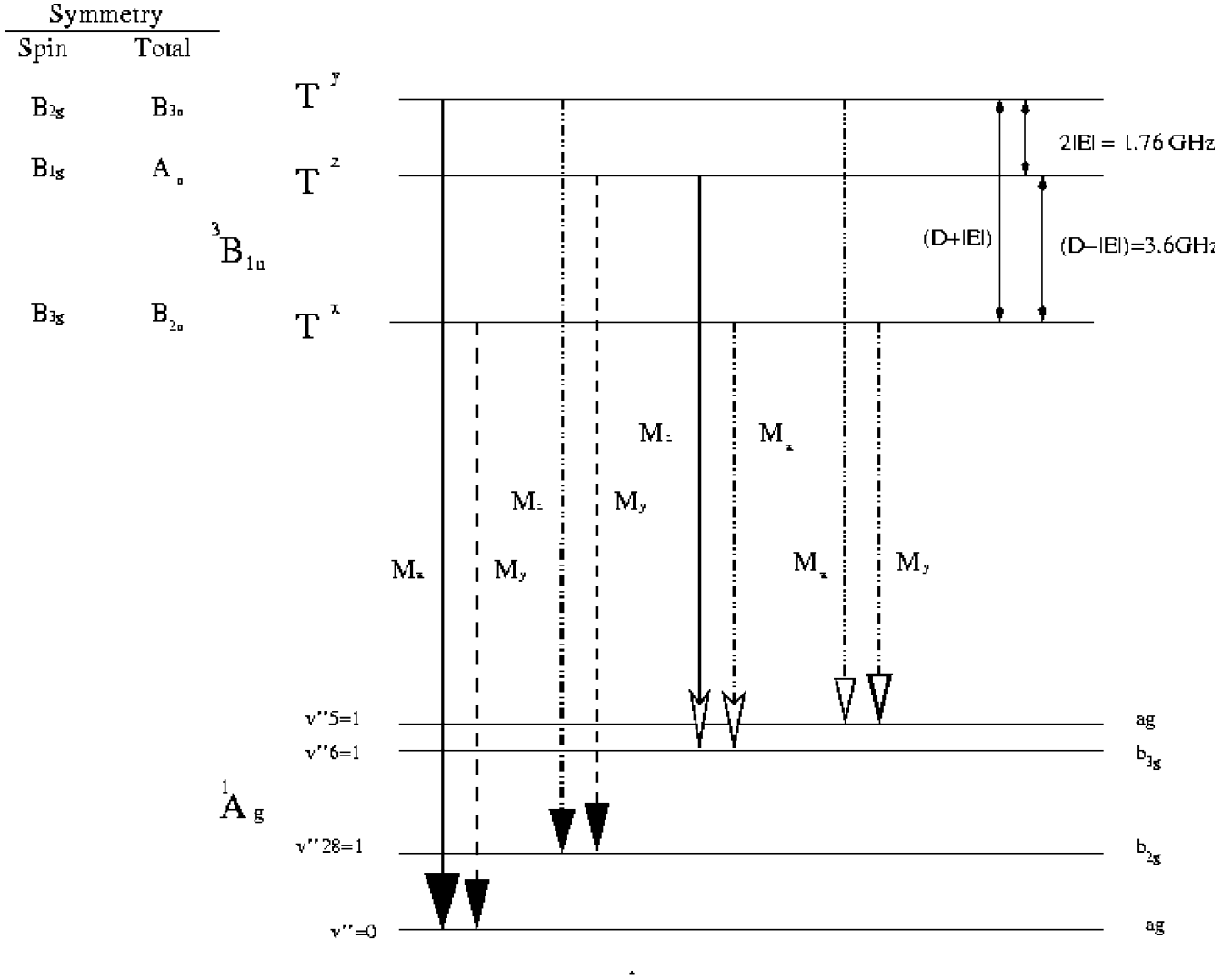

Fig. 5. Scheme of the phosphorescence process from different spin sublevels to the vibrational levels in the ground state

MIDP signals produced 100 ms after the excitation cutoff by irradiating with microwaves resonant with the $T^y \leftrightarrow T^z$ transition. The T^y spin sublevel decays very fast, while the other two sublevels T^x and T^z, remain populated (they have longer lifetimes). The population of the T^y sublevel is completely exhausted after 100 ms and the $T^y \leftarrow T^z$ microwave pumping produces an MIDP signal which is a pure $T^y \rightarrow S_0$ phosphorescence emission. The vibronic band $a_g(\nu_5)$ is very intense in the T^y spectrum, while it is weak in the MIDP spectra detected for the other two spin sublevels T^x and T^z. The T^x and T^z phosphorescence spectra are obtained by recording the tail portions of the emission decay at a longer time (150 ms) [21, 22].

The T^z spin sublevel is dark ($\kappa^z = 0$) for the free PDCB molecule of D_{2h} symmetry. The value of κ^z is obtained small but nonzero in ODMR measurements [21] and depends strongly on the host crystalline system. In deuterated PDCB the relative radiative rate constants κ^x and κ^z increase (the latter much more). The same trend is prominent for PDCB trapped in a *P*-dibromobenzene host crystal [21], which is a pure indication of the external heavy-atom effect. The κ^x and κ^z constants for the trap in the neat crystal seem to have an influence from other sources in addition to the external heavy-atom effect. As a possible cause a rotation of the trap molecules has been proposed [21].

The other component of the close-lying doublet for the (0,0 + 1580 cm^{-1}) vibronic bands, namely the $b_{3g}(\nu_6)$ mode, is found to be very active in our calculation, as it is in the ODMR and MIDP experiments [15, 21, 22]. The phosphorescence intensity originating from T^y with *x*-polarization (M_x) and from T^x with *y*-polarization (M_y) spin sublevels is not changed upon excitation of this vibration (the derivatives are zero, thus the vibronic activity is low) but there occurs a new emission from the T^z and T^x sublevels which were dark for the $a_g(\nu_5)$ vibrational mode. In the T^z spin sublevel, the derivative, $\partial M(T^z)/\partial Q_{1692} = 8.75\times10^{-6}$ is one of the highest obtained in our calculations among all vibrations which are allowed by the symmetry selection rules for the ${}^3B_{1u} \rightarrow {}^1A_g(\nu')$ phosphorescence. The corresponding transition moment is finally $M_x(T^z) = 39.75\times10^{-6}$ au and $\kappa^z = 0.0582\ s^{-1}$.

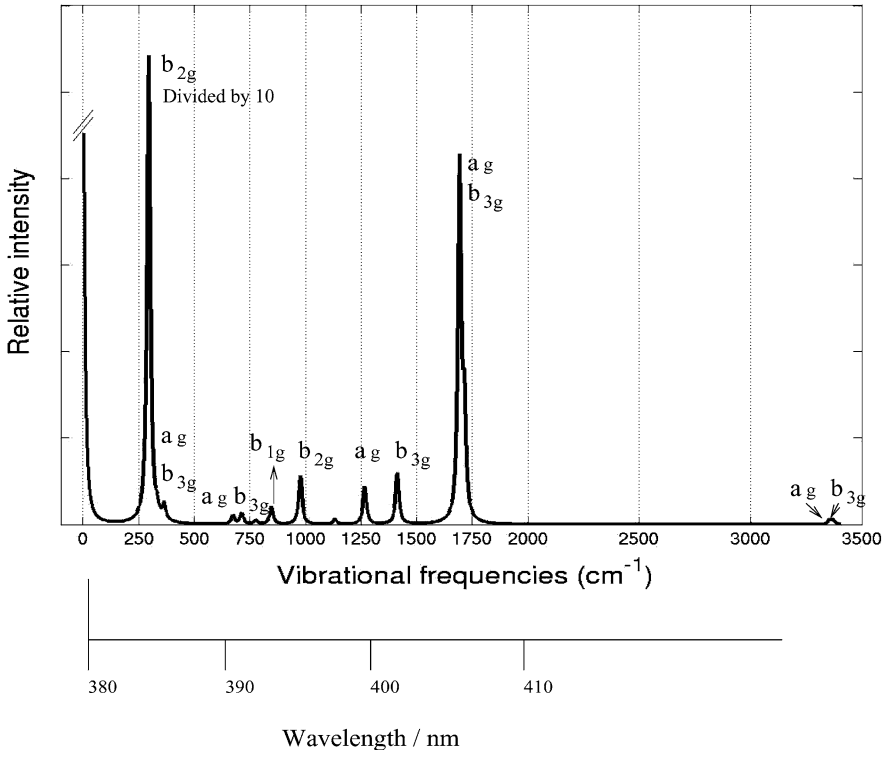

Fig. 6. Simulated vibrational phosphorescence spectra. The fundamental bands in the spectrum are assigned. The more intense vibrational band ($b_{2g}\nu_{28}$) is reduced 10 times. The 0-0 band is cut down

In the T^x spin sublevel spectra, the contribution from the $b_{3g}(\nu_6)$ vibronic band is smaller and the final transition moment, $M_z(T^x) = 11.35\ 10^{-6}$ au produces a small value of the rate constant, $\kappa^x = 0.0048\ s^{-1}$. The ratio of the rate constants in the $b_{3g}(\nu_6)$ vibronic band (0,0 + 1692 cm^{-1}) in our calculation is $\kappa^x/\kappa^z = 0.08$ for both active spin sublevels, which corresponds to $\kappa^x/\kappa^z = 0.24$ for the band at 0,0 + 1573 cm^{-1} in the experimental data in a *p*−xylene host crystal. In the neat crystal this ratio is 0.045 and it is 0.02 in the deuterated host [21].

For the other modes of the a_g symmetry it is remarkable that the $a_g(\nu_{10})$ mode, present at 0,0 + 1266 cm^{-1} in our calculation, is associated with considerable intensity in the simulated spectra with the contribution from the T^y, spin sublevel, $M_x(T^y) = -13.13\ 10^{-6}$ au, see Table 4 and Fig. 6. It is present in the experimental spectrum at 0,0 + 1074 cm^{-1} for PCDB d_4 in a *p*−xylene matrix [21] with similar relative phosphorescence intensity.

Among the b_{3g} modes, another prominent feature with a visible intensity is given by the vibronic $b_{3g}(\nu_9)$ band at (0,0 + 1413 cm^{-1}) in our calculated spectra with a transition moment $M_x(T^z) = 15.54 \times 10^{-6}$ au. It is present in the experimental spectrum [21], and is assigned at 0,0 + 1297 cm^{-1} in the phosphorescence spectra of PCDB in a *p*−xylene matrix.

Finally, in the high-energy region of the spectrum two modes are present with low intensity. They were well studied in previous experimental works. These modes are $b_{3g}(\nu_3)$ and $a_g(\nu_1)$; they have similar values of the transition moments from all the spin sublevels and very close vibrational frequencies, $\nu_1 = 3371\ cm^{-1}$ and $\nu_3 = 3354\ cm^{-1}$, assigned to the stretching symmetric and antisymmetric movement of the C–H vibration in PDCB.

The only transition of b_{1g} symmetry, which appears in the experimental spectrum at 0,0 + 640 cm^{-1} with strong relatively intensity, is of special interest. It has been assigned to the b_{1g} fundamental because of the negative sign of the $T^z \leftrightarrow T^y$ transition moment in the PMDR spectra [21]. The b_{1g} (ν_{19}) mode due to the out-of-the-plane stretching of the C–C bond in our calculation is present at 846 cm^{-1}. It has a value of $\kappa^z = 0.0149\ s^{-1}$ with a contribution from $M_z(T^z)$ of 2.00×10^{-6} au. The b_{1g} vibrational mode has another contribution from the spin sublevel $M_x(T^x) = 8.01 \times 10^{-6}$ au with $\kappa^x = 0.0024\ s^{-1}$, and one more small contribution from $M_y(T^y) = 3.13 \times 10^{-6}$ au with $\kappa^y = 0.0149\ s^{-1}$. This band possesses a smaller phosphorescence intensity from the T^x spin sublevel in comparison with the $b_{3g}(\nu_6)$ band at the same spin sublevel, [$M_z(T^x) = 11.35 \times 10^{-6}$ au]. This contribution is not as large as in the experimental data recorded by Iwasaki et al. [22], and the contribution of T^z is larger in the b_{3g} modes as is indicated in the sublevel phosphorescence spectra.

The low-frequency region of the spectrum presents several vibronic bands at about 290-360 cm^{-1}, Tables 4, 5 and 6. The a_g (ν_{27}) band at 334 cm^{-1} corresponds to the vibration of the C–Cl bond in the molecular plane, in which the T^y spin sublevel has the main contribution, Table 4. It corresponds to the 333-cm^{-1} feature in the experimental spectrum in a neat crystal, and to the 337-cm^{-1} feature in deuterated PDCB [21]. In our calculated spectra this mode appears with a major contribution from the T^y spin sublevel with $\kappa^y = 0.0015\ s^{-1}$ and $M_x(T^y) = 6.39 \times 10^{-6}$ au. The second mode in this area is a b_{3g} mode (ν_{26}) due to the bending movement of the C–Cl bond in the molecular plane, computed to be 364.81 cm^{-1}. In the Raman spectrum it occurs at 350 cm^{-1}, and at 355 cm^{-1} in the neat crystal matrix (Table

1). The b_{3g} modes are forbidden in emission from the T^y spin sublevel in the D_{2h} point group, and only contributions from the other spin sublevels could allow the S→T transition. At the same time, vibronic transitions from the T^x and T^z levels for the b_{3g} (ν_{26}) mode are not very active, $M_z(T^x) = M_x(T^z) = 6.11 \times 10^{-6}$ au, and $\kappa^z = \kappa^x = 0.0014\ s^{-1}$, Table 5.

A very strong vibronic band corresponding to the b_{2g} (ν_{28}) mode near (0,0 + 300 cm^{-1}) is present in both the experimental and the simulated spectra. It has the largest derivative and the largest transition moment from the T^y spin sublevel in comparison with all the other vibrational modes, $M_z(T^y) = 136\ 10^{-6}$ au, $\kappa^y = 0.6831\ s^{-1}$. It is almost comparable to the transition moment of the 0,0 band [$M_x(T^y) = 148 \times 10^{-6}$ au]. This band, which has an additional contribution from the T^z spin sublevel with M_y polarization, $M_y(T^z) = 20.40 \times 10^{-6}$ au, $\kappa^z = 0.0154$ s^{-1}, is present at 295.01 cm^{-1} in our computed spectra, and corresponds to the bending of the C–Cl bond out of the molecular plane. In the experimental spectra the band is present at about (0,0 + 308 cm^{-1}); at 306 cm^{-1} in the Raman spectrum and at 314-cm^{-1} in the neat crystal matrix. It has been assigned as being due to the progression forming the b_{2g} vibration (C–Cl out-of-plane bending). The (0,0 + 308-cm^{-1}) band is the strongest band in the spectrum of PDCB in the deuterated crystal, in *p*-xylene and in a benzene host [21], while in the phosphorescence spectrum of PDCB in *p*−dibromobenzene it exhibits much weaker intensity than the 0-0 band. This is a clear indication of the destructive external heavy-atom effect in the T→S transition which depends only on the electronic SOC perturbation and does not depend on the intramolecular vibronic interactions.

Other less intense modes along the b_{2g} symmetry should be considered in our theoretical spectra. First, the vibronic band b_{2g} (ν_{17}) appears at about (0,0 + 976 cm^{-1}), corresponding to the experimental peak at 970 cm^{-1} in *p*−dibromobenzene, and at 938 cm^{-1} in *p*-xylene and in the neat crystal matrices. It has a quite large transition moment from the T^z spin sublevel, $M_y(T^z) = 14.95 \times 10^{-6}$ au, and $\kappa^y = 0.0418\ s^{-1}$. The second b_{2g} vibronic band appears softly in emission at 689 cm^{-1}, in the Raman spectrum, and at 694 cm^{-1} in p-xylene and 691 cm^{-1} in neat crystal matrices [21]. We have assigned it to $b_{2g}(\nu_{21})$, $\nu = 713\ cm^{-1}$. It is less intense than the other two b_{2g} bands, but still has some visible intensity in our simulated phosphorescence spectrum $M_z(T^y) = 5.69 \times 10^{-6}$ au, $\kappa^y = 0.1194$ s^{-1}, Table 6.

4 Conclusions

This paper presents results for vibronic analysis of the phosphorescence spectrum ($^3B_{1u} \rightarrow {}^1A_g$) of PDCB by means of MCSCF calculations and QR methodology. The calculations were carried out for all allowed vibrational modes of the $S_0(\nu_i)$ ground state in order to study the vibronic spin-forbidden transitions $T_1^k \rightarrow S_0(\nu_i)$ and the vibrational profile of the phosphorescence spectra. The information gained from such calculations concerns polarization directions, oscillator strengths, radiative lifetimes, molecular geometry in the ground and excited states, vibrational assignments of the bands in the spectrum, and excitation energies for the triplet states. These quantities either refer to values averaged over triplet states or to specific triplet-state spin sublevels. We also performed calculations of ZFSs and NQC constants. Thus, we made a full theoretical assignment of the vibronic phosphorescence spectrum specific for each triplet-state spin sublevel which has previously been recorded by the phosphorescence microwave double resonance method [4].

The reduction of the NQC constant along the $S_0 \rightarrow T_1$ excitation was studied assuming D_{2h} and C_{2h} symmetries. The results using D_{2h} symmetry are in concordance with the results obtained using lower symmetry, and with experimental data. Thus, to a first approximation the D_{2h} symmetry for the lowest triplet state is able to adequately describe the molecular properties. The optimized geometry of the lowest triplet state has a chlorine atom out of the benzene molecular plane, while the other chlorine atom is lying in this plane. Such a geometry will give different values for the NQC constants of the chlorine atoms. This fact is not in agreement with the experimental results [21], but can probably be explained by this distortion not being energetically allowed in the matrix when the crystal force fields prohibit the molecule from reaching the most favorable structure.

One of the most intense and controversial vibronic bands [21,4], present at about 1580 cm^{-1} in the experimental spectrum, is shown here to be the result of a combination of two different vibrations. The calculations indicate that the vibrational a_g (ν_5) mode at 1713.61 cm^{-1} and the b_{3g} (ν_6) mode at 1692.73 cm^{-1} are responsible for this intense transition in the phosphorescence spectrum, originating from the most active spin sublevel (T^y) in agreement with the PMDR data. Other particular features appear in the low-vibrational-frequency area of the spectrum at about 300 cm^{-1}, with several vibrational modes present. In this work we assigned these features to the vibrational b_{2g} (ν_{28}) C–Cl bending out-of-the-plane mode, as the most intense vibronic transition in this region. However, it appears that the intensity of this band is overestimated by the MCSCF-QR calculations. The remaining vibrational bands originating from different modes with less intensity were also presented and discussed in this work. The simulated vibronic spectrum and the molecular geometries were described. All the relative vibronic band intensities are in good qualitative agreement with experimental spectra.

From the present applications of ab initio QR techniques to the vibronic phosphorescence spectrum of PCDB we learn a unique lesson about the close connections between internal magnetic interactions and vibrational movements in molecules. An analysis of these connections permits us to understand the origin of changes in phosphorescence intensity induced by microwaves in the sense that specific ZFS spin transitions produce enhancements of particular vibronic modes. Thus, vibrations of large amplitude which lead to

chemical bond cleavage (the starting point of chemical reactivity) can induce a strong spin selectivity of the triplet state sublevels with respect to the intersystem crossing and with respect to other spin-dependent photochemical and photophysical processes. This can give rise to external magnetic field effects and to chemically induced spin polarization. Direct ab initio calculations of spin-vibronic effects in transition states or in the singlet–triplet crossings can provide more in-depth views on such phenomena.

Acknowledgments O. R.-P. would like to thank the European MOLPROP network for support. The authors thank Alexander Baev for fruitful discussions. This work was supported by the Swedish Royal Academy of Science (KVA).

References

1. Schmidt J, van der Waals JH (1969) Chem Phys Lett 3: 546
2. Castro G, Hochstrasser RM (1967) J Chem Phys 46: 3617
3. McGlynn SP, Azumi T, Kinoshita M (1969) Molecular spectroscopy of the triplet state NJ Prentice Hall Engelwood cliffs
4. Buckley MJ, Harris CB (1972) J Chem Phys 56: 137
5. El-Sayed MA, Ramsey AD, Ramsay DA (1972) In: MTP international review of science, spectroscopy, Butterworth, London (eds) pp 119
6. Minaev BF (1979) Fiz Mol Nauk Dumka, Kiev 7: 34
7. Turro N, Devaquet A (1975) J Am Chem Soc 97: 3859
8. Minaev BF, Lunell S (1993) Z Phys Chem 182: 263
9. Minaev BF Ågren H (1999) J Mol Catal A 149: 179
10. Wu J, Baumann D, Steiner UE (1995) Mol Phys 84: 981
11. Minaev BF, Ågren H (1995) Collect Czech Chem Commun 60: 339
12. Prabhakar R, Siegbahn P, Minaev B, Ågren H (2002) J Phys Chem B 106: 3742
13. Terenin AN (1943) Acta Physicochim. URSS 18: 210
14. Albrecht AC (1963) J Chem Phys 38: 354
15. Buckley MJ, Harris CB, Panos RP (1972) J Am Chem Soc 94: 3693
16. Minaev BF, Knuts S, Ågren H, Vahtras O (1993) Chem Phys 175: 245
17. Knuts S, Minaev BF, Ågren H, Vahtras O (1994) Theor Chim Acta 87: 343
18. Minaev BF (1971) Izv Vyssh Ucheebn Zaved Fiz 5: 93
19. Hochstrasser RM, Lin TS (1968) J Chem Phys 49: 4929
20. Kothandaraman G, Tinti DS (1973) Chem Phys Lett 19: 225
21. Kinoshita M, Goto N, Iwasaki N (1983) Bull Chem Soc Jpn 56: 2591
22. Iwasaki N, Goto N, Kinoshita M (1983) Chem Phys 81: 449
23. Rubio-Pons O, Loboda O, Minaev BF, Schimmelpfenning B Vahtras O, Ågren H (2003) Mol Phys 101: 2103
24. van Egmond J, van der Waals JH (1973) Mol Phys 26: 1147
25. Ågren H, Vahtras O, Minaev BF (1996) Adv Quantum Chem 27: 71
26. Vahtras O, Minaev BF, Loboda O, Ågren H, Ruud K (2002) Chem Phys 279: 133
27. Helgaker T, Jensen HJA, Jørgensen P, Olsen J, Ruud K, Ågren H, Auer AA, Bak KL, Bakken V, Christiansen O, Coriani S, Dahle P, Dalskov EK, Enevoldsen T, Fernández B, Hättig C, Hald K, Halkier A, Heiberg H, Hettema H, Jonsson D, Kirpekar S, Kobayashi R, Koch H, Mikkelsen KV, Norman P, Packer MJ, Pedersen TB, Ruden TA, Sánchez A, Saue T, Sauer SPA, Schimmelpfennig B, Sylvester-Hvid KO, Taylor PR, Vahtras O (2001) Dalton a molecular electronic structure program, release 1.2
28. Langhoff SR, Davidson ER, Kern CW (1975) J Chem Phys 63: 4800
29. Lide DR (1993) CRC handbook of chemistry and physics. 73rd edn. CRC Boca Raton
30. Langhoff SR, Davidson ER (1976) J Chem Phys 64: 4699
31. Klotz R, Marian CM, Peyerimhoff SD, Hess BA, Buenker RJ (1984) Chem Phys 89: 223
32. Yarkony DR (1992) Int Rev Phys Chem 11: 195
33. Schimmelpfenning B (1996) AMFI, an atomic mean-field spin-orbit integral program Stockholm University Sweden
34. Roche M, Jaffé H (1974) J Chem Phys 60: 1193
35. Herzberg G, Teller E (1933) Z Phys Chem B21: 410
36. Minaev BF, Knuts S, Ågren H, Vahtras O (1993) Chem Phys 175: 245
37. Widmark P-O, Malmqvist P-Å, Roos BO (1990) Theor Chim Acta 77: 291–306
38. Frisch MJ, Trucks GW, Schlegel HB, Scuseria GE, Robb MA, Cheeseman JR, Zakrzewski VG, Montgomery JA Jr, Stratmann RE, Burant JC, Dapprich S, Millam JM, Daniels AD, Kudin KN, Strain MC, Farkas O, Tomasi J, Barone V, Cossi M, Cammi R, Mennucci B, Pomelli C, Adamo C, Clifford S, Ochterski J, Petersson GA, Ayala PY, Cui Q, Morokuma K, Malick DK, Rabuck AD, Raghavachari K, Foresman JB, Cioslowski J, Ortiz JV, Baboul AG, Stefanov BB, Liu G, Liashenko A, Piskorz P, Komaromi I, Gomperts R, Martin RL, Fox DJ, Keith T, Al-Laham MA, Peng CY, Nanayakkara A, Gonzalez C, Challacombe M, Gill PMW, Johnson BG, Chen W, Wong MW, Andres JL, Head-Gordon M, Replogle ES, Pople JA (1998) Gaussian 98 (revision A.x). Gaussian, Pittsburgh, PA
39. Muldahmetov ZM, Minaev BF, Ketsle GA (1983) Optical and Magnetic properties of the triplet State Nauka Alma Ata (in Russian)
40. Hochstrasser RM, Lin TS (1970) J Chem Phys 53: 2676
41. Lucken EAC (1969) Nuclear quadrupole coupling constants. Academic, New York